RSC Advances

ROYAL SOCIETY OF CHEMISTRY

www.rsc.org/advances

Cite this: DOI: 10.1039/c0xx00000x

www.rsc.org/xxxxxx

ARTICLE TYPE

One-step synthesis of nanohybrid carbon dots and TiO_2 composites with enhanced ultraviolet light active photocatalysis

Fan Li, Feng Tian,* Changjun Liu, Zheng Wang, Zhenjie Du, Ruixin Li, Li Zhang

Received (in XXX, XXX) Xth XXXXXXXXX 20XX, Accepted Xth XXXXXXXXX 20XX

DOI: 10.1039/b000000x

Nano-hybrid composites of carbon dots (CDs) and titanium dioxide (TiO_2) were fabricated by a designed one-step solvothermal method. The crystallinity of TiO_2, morphologies and ingredients of the CDs-TiO_2 composites could be adjusted by the reaction time. Furthermore, the measurements of photo-degradation on methyl blue (MB) showed excellent photocatalytic activity of the CDs-TiO_2 composites under ultraviolet (UV) light irradiation, which was much higher than that of commercial Degussa P25. However, C-TiO_2 composites, which were produced from the CDs-TiO_2 composites by a further calcination, showed a more excellent photocatalytic activity on the photo-degradation of methyl orange (MO) and rhodamine B (RB).

Introduction

Due to its low cost, high chemical stability and non-toxicity, titanium dioxide (TiO_2) has been widely used as one of the most promising photocatalysts.[1] The photocatalytic activity of TiO_2 originates from the photo-generated charge carriers (electrons and holes) which are strong reducing and oxidizing agents. However, the wide band gap (3.2 eV for anatase and 3.0 eV for rutile) of TiO_2 limits its response to the ultraviolet (UV) light only, leaving 95-97% energy of the whole solar spectrum unusable. Great efforts have been made to modify TiO_2 so as to improve its photo response capability. A variety of effective approaches, such as coupling with other semiconductor materials,[2-4] doping with metal ions,[5-9] sensitization using a dye,[10-12] compounding with noble metal (deposition or encapsulation)[13-15] and doping with nonmetal elements,[16-24] have been explored to enhance the photocatalytic performance of TiO_2 under visible light, all of which are based on the formation of intermediate energy levels in the band gap. Among the doping processes using nonmetal elements, Asahi et al. pioneered the nitrogen doping with TiO_2, which promoted visible light activity of TiO_2 in photodetoxification.[17] Subsequently, other nonmetal elements, such as carbon,[18,19] sulfur,[20] fluorine[21], boron[22] and hydrogen[23,24], were employed in diverse doping studies on TiO_2 as well.

In most cases TiO_2 could show photocatalytic activity under visible light after doping processes. However, the recombination of photo-generated carriers was accelerated on account of numerous recombination centers brought by the introduction of impurities and defects. Therefore, it is better to transfer the photo-generated electrons off TiO_2 to retard the recombination. Taking this into account, carbon materials have great advantages among all candidate materials, owing to their excellent electronic conductivity, electron-storage capacity, absorbency of visible light and chemical stability. Graphene[25] and carbon nanotubes (CNT)[26] had been used to suppress the recombination of photo-generated carriers. But the limited contact between graphene (or CNT) and TiO_2 nanoparticles were adverse to the electrons shift from TiO_2 to carbon materials. Choi et al.[27] designed a core-shell photocatalyst of TiO_2@reduced graphene oxide (RGO), whereas the RGO shell would probably hinder the degradation of organic pollutants. The C/TiO_2 photocatalysts with ordered nanostructures and pronounced photocatalytic activity under visible light were obtained by direct carbonization of block copolymer templates.[28] Latter the composites of amorphous carbon and TiO_2 also showed improved photocatalytic activities.[29,30] However, the best performance of these pholocatalysts could be achieved only when an anneal process was carried out to etch partial carbon content.

Carbon dots (CDs), emerged as a novel and eco-friendly carbon nanomaterial, has attracted considerable attention due to their versatile preparation routes, better biocompatibility and particularly tunable photoluminescence (PL).[31] Lee et al. firstly proved the availability of TiO_2/CDs hybrids for the efficient photo-degradation of methyl blue.[32] Then Ho et al. found the H_2 evolution rate of TiO_2/CDs nanocomposites was 9.7 times higher than that of bare TiO_2.[33] Likewise, the photocatalytic rate of alkylated graphene quantum-P25 nanocomposites was much higher than that of pure P25 under visible light.[34] Recently, TiO_2 with various microstructures, such as nanosheet,[35] nanorod,[36] nanowire,[37] nanotube,[38] hollow microspheres[39] and nanorod spheres[40], were explored to combined with CDs as well, all of which showed enhanced photocatalytic activity. However, ready-made TiO_2 materials or special efforts on TiO_2 preparation were necessary in most of previous doping studies. In fact, the N-doped CDs themselves have showed excellent photocatalytic property in the photo-degradation of methyl orange under visible light.[41] Latter Kang et al. confirmed that graphite-derived CDs could be used for photoelectrochemical hydrogen generation.[42] It is indicated that CDs are promising candidates for photocatalytic

applications.

In this work, we designed a one-step solvothermal process to fabricate nanohybrid composites of CDs and TiO_2 in situ. The mixture of citric acid and tetrabutyl titanate dissolved in ethanol acted as carbon source and TiO_2 precursor separately. The H_2O generated from the dehydration and impartial carbonization of citric acid was immediately utilized to initiate the hydrolysis of tetrabutyl titanate, which was turned into the earliest sol-gel TiO_2 and final TiO_2 nanocrystal. In this way it is expected to realize a maximum contact between the as-prepared CDs and TiO_2 in the final composites for the benefit of an enhanced photocatalytic performance. The possible formation process of the CDs-TiO_2 composites was illustrated in Scheme 1. Furthermore, methyl blue (MB), methyl orange (MO) and rhodamine B (RB) were chosen to test the photocatalytic activity of the nanohybrid CDs-TiO_2 composites under UV light irradiation.

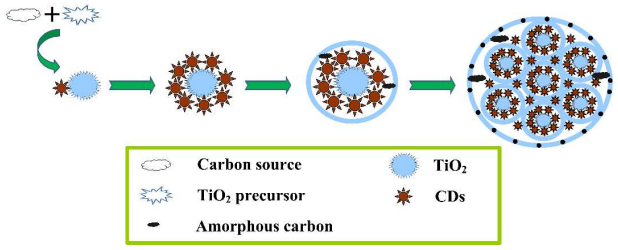

Scheme 1 Schematic illustration of the formation process of the CDs-TiO_2 composites in situ.

Experimental section

Chemicals and reagents

Citric acid (CA, 99.5%) was purchased from Alfa Aesar. Methylene blue (MB, 98.5%), methyl orange (MO, 99.7%) and rhodamine B (RB, 99%), tetrabutyl titanate (TBT, 99%), triethanolamine (85%) and ethanol (99.7%) were obtained from GuangFu Technology Development CO, LTD. All other reagents were of analytical grades and used without further purification.

Preparation

Tetrabutyl titanate was used as the TiO_2 source. Typically, 2 g CA was dissolved in 60 ml ethanol followed by an addition of 10 ml TBT in succession to form a colorless, transparent and homogeneous solution. Then, a certain amount of TEA was added dropwise into the solution under vigorous stirring for 30 min. The mixed solution was placed into a 100 ml stainless steel autoclave with a Teflon liner. The autoclave was incubated at 200 ºC for t h (t=3, 6, 9 or 12) and then cooled to ambient temperature. After the solvothermal reaction, the white precipitates were filtrated and washed with ethanol and water in turns for five times. The obtained CDs-TiO_2 composites (marked as C-3, C-6, C-9 and C-12 orderly) were dried at 80 ºC in a vacuum oven overnight and then ground to fine powders with an agate mortar. Pure CDs were prepared following the same way above except the addition of TBT. In order to regulate the components of the obtained CDs-TiO_2 composites, another 2 h calcination under different temperature (400 ºC, 450 ºC, 500 ºC and 550 ºC, separately) in air were carried out and the final samples (C-TiO_2 composites) were named C-400, C-450, C-500 and C-550 correspondingly.

Characterizations

UV-Vis absorption was measured on a DR 5000 UV-Vis spectrophotometer (HACH, America). PL emission measurements were performed using a FLS920 fluorometer (Edinburgh Instruments, Britain). The normalized spectrum was obtained by divided each intensity of the PL spectrum by the maximum value of its own. The morphology and microstructure of the samples were examined by scanning electron microscopy (SEM) on a LEO 1530VP scanning electron microscope with an acceleration voltage of 20 kV. The obtained composites and pure CDs were further examined by high-resolution transmission electron microscopy (HRTEM) on a Philips Tecnai G2 F20 microscope (Philips, Netherlands) with an accelerating voltage of 200 kV. The samples for HRTEM were made by dropping an aqueous solution onto a 300-mesh copper grid coated with a lacy carbon film. The fourier transform infrared (FTIR) spectra of CDs were measured on a Nicolet 380 spectrometer (Thermo, America). The surface states and composition of the composites were measured on a Kratos AXIS Ultra DLD X-ray Photoelectron Spectroscopy (XPS, Shimadzu, Japan). X-Ray diffraction (XRD) profiles of the prepared samples were recorded on a Rigaku-D/MAX 2500 diffractometer (Rigaku, Japan) equipped with graphite monochromatized CuKα (λ=0.15405 nm) radiation at a scanning speed of 4° min^{-1} in the range from 10° to 70°. The Brunauer-Emmett-Teller (BET) specific surface areas of the composites were calculated using adsorption data in the relative pressure range from 0.04 to 0.32, while the Barret-Joyner-Halenda (BJH) pore size distribution was determined from the desorption isotherms. The thermogravimetric curves were finished from 50 ºC to 650 ºC under N_2 with a same heating rate (10 ºC per min) on a thermo gravimetric analyzer (Mettler).

Measurements of photocatalytic activity

The photocatalytic activity of all samples was tested under UV light. MB solution with different concentrations (0-10 ppm) was prepared in water. Typically, 10 mg powder samples were suspended in 8 ml MB solution followed by 10 min vortex and 120 min vibration in the dark to reach the adsorption-desorption equilibrium between MB and photocatalysts before irradiation. Then the above reaction system placed in a quartz cuvette was exposed to UV light with a wavelength of 254 nm and a power of 8 W (Spectroline XLE-1000/F, UV CROSSLINKER) at room temperature. Without stirring, the suspension was taken out at regular intervals and centrifuged at 5000 rpm for 10 min, and then the supernatant solution was analyzed using a UV-Vis absorbance spectroscopy. The photo-degradation measurements on MO and RB were executed in the same way.

Results and Discussion

XRD was used to investigate the possible constituents and crystalline phase of the samples prepared under different conditions. As shown in Fig. 1, it is easy to find the existence of TiO_2 as an imperfect crystal of anatase. Meanwhile, the XRD patterns differed from each other but with a regular tendency. The diffraction peak of sample C-3 was broad, which meant an unformed crystalline phase. But with prolonged reaction time, the diffraction peaks attributing to anatase TiO_2 became visible and acute gradually from sample C-6 to C-12. It should be pointed out

that these peaks were comparatively weak due to the ultra small size of the TiO_2 crystallites which were finely doped with the carbon materials (CDs) in the samples. As an amorphous carbon, the as-prepared pure CDs showed a very weak and broad peak between 20° to 30° (Shown in Fig. S1), which might have been covered by the lineshape belonging to TiO_2 grains in the XRD patterns of the CDs-TiO_2 composites. The average grain sizes of TiO_2 measured with Scherrer equation increased from 8.1 nm of sample C-6 to 11.9 nm of sample C-12. More details were listed in the Table S1. It had been reported that carbon deposition had a depression effect on the grain growth of TiO_2,[43] meanwhile it's known that crystal growth could develop gradually with prolonged heating time. So there was a competition for the development of TiO_2 grains in the solvothermal process. However, after a further calcination merely at 400°, rutile TiO_2 was found, together with the predominant anatase TiO_2 (Fig. S2). The proportion of rutile TiO_2 increased quickly with enhanced annealing temperature, and the ratio of anatase/rutile in sample C-450 was very close to that of commercial Degussa P25.

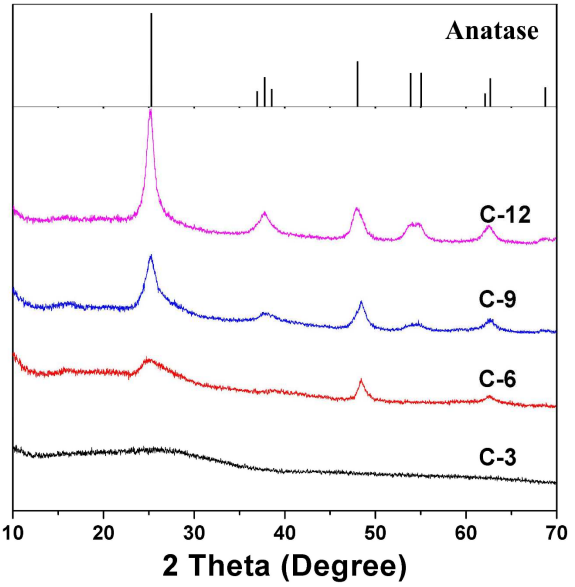

Fig. 1 XRD patterns for the CDs-TiO_2 composites prepared with different heating time.

The microstructures and morphologies of as-prepared CDs-TiO_2 composites were probed using SEM (Shown in Fig. 2). In the panoramic view, the samples were all microspheres with diameter no more than 10 μm. But the surface morphologies differed greatly from sample C-3 (Fig. 2a) to sample C-12 (Fig. 2b). Sample C-3 possessed a rather smooth surface (Fig. 2d). But with prolonged heating time, the surface of microspheres became more and more rough. The high magnification SEM images (Fig. 2e) revealed that the surface of sample C-12 was overspread with small particles with an average diameter about 30 nm. After a further calcination under 450 ºC, most microspheres of sample C-450 broke (Fig. 2c), and the inner morphologies were exposed. Similarly, the high magnification SEM images (Fig. 2e) showed that the inner space of microspheres was also filled fully with nanoparticles. Taking the surface structure into account synchronously, it was easy to speculate that the basic unit of the microspheres was the observed nanoparticles, which further joined together to form the final microspheres. While CDs were produced from incomplete carbonization of the precursor molecules. Therefore, the basic nanoparticles were probably composed of CDs, TiO_2 nanocrystals and a very few residues of partially reacted precursor molecules. Meanwhile it's just the reason why the surface of microspheres became rough with prolonged heating time. The remnant precursor molecules among the nanoparticles continued to be carbonized or transformed into TiO_2 nanocrystal, bringing about a lot of mesopores or even macropores in the microspheres and leaving a tough irregular surface or some broken microspheres (Fig. S3). But when a further calcination was applied on the CDs-TiO_2 composites, CDs and almost all the residual precursor molecules were consumed, the linkages among the basic nanoparticles were destroyed completely, finally leading to the fact that a majority of microspheres broke. It was worthwhile to note that the nanoparticles undergone a treatment of calcination became smaller with a careful examination, which indirectly indicated that CDs and TiO_2 were hybridized finely and evenly in the microspheres of CDs-TiO_2 composites.

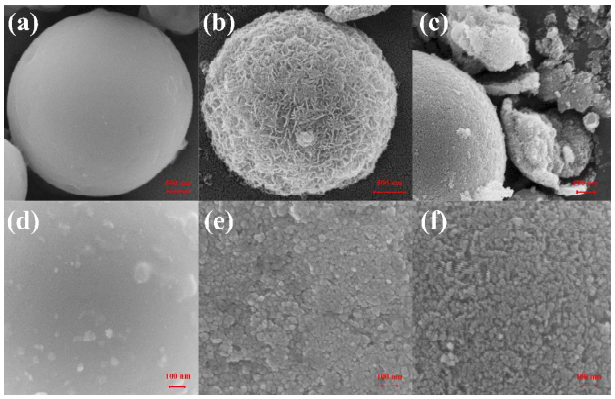

Fig. 2 SEM micrographs of the as-prepared composites (a), (b) and (c): low magnification images of sample C-3, C-12 and C-450 (scale bars: 500 nm); (d), (e) and (f): high magnification images of the surface structures of sample C-3, C-12 and C-450 (scale bars: 100 nm).

HRTEM analyses were conducted to further study the microstructure of the obtained composites. It's confirmed that both sample C-9 and C-450 were composed of nanoparticles (Fig. 3a and Fig. 3c). And the high magnification HRTEM images of sample C-9 showed clear lattice fringes of the nanocrystals with an interplanar spacing of 0.35 nm around, which matched well with the (101) plane of anatase TiO_2. The pure CDs were distributed well with an average diameter of 5 nm around, in accordance with the poor crystallinity (Shown in Fig. S4). In Fig. 3b, inside the red dotted boxes were CDs, which were linked to the TiO_2 nanocrystals. Few CDs were found at the TiO_2 surfaces of sample C-450 (Fig. 3d). Besides anatase TiO_2, HRTEM images revealed another TiO_2 nanocrystal, the interplanar spacing of which was about 0.32 nm, belonging to the (110) plane of rutile TiO_2. The HRTEM analyses were correspondent with the XRD results. It can be concluded from Fig. 3 that sample C-9 was composed of TiO_2 nanocrystals and CDs, with few partially reacted precursors being deposited on the surface and between them. As to sample C-450, TiO_2 nanocrystals with two structures, few CDs and the carbon matrix (amorphous) produced from the previous residues constituted the whole composites.

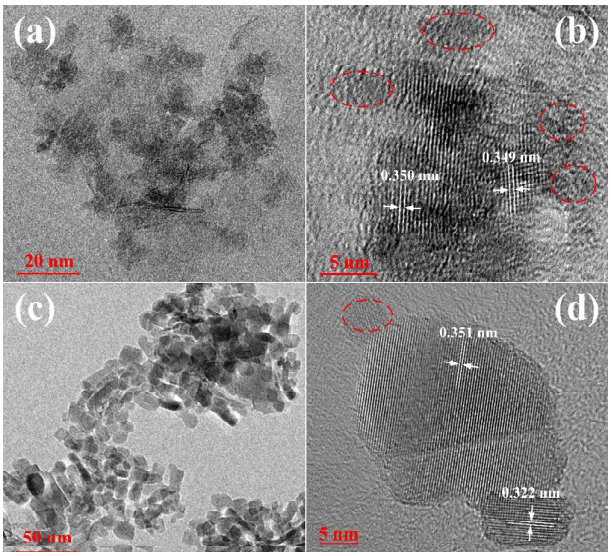

Fig. 3 HRTEM images of sample C-9 (a and b) and C-450 (c and d).

The thermogravimetry results (Shown in Fig. S5) revealed that the weight loss of sample C-9 was exactly similar to that of pure CDs, while the thermogravimetric curves of sample C-450 remained nearly unchanged. This result reconfirmed that the further calcination mainly consumed CDs and previous unreacted precursors in sample C-9, which probably converted the CDs-TiO_2 composites into C-TiO_2 composites.

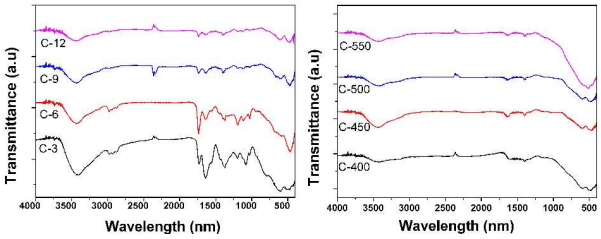

Fig. 4 FTIR spectra of the as-prepared CDs-TiO_2 composites (left) and C-TiO_2 composites (right).

The FTIR spectra were shown in Fig. 4, the trend of characteristic peaks for CDs-TiO_2 composites that only suffered a solvothermal process was evident with prolonged heating time, while there were nearly no difference for the C-TiO_2 composites. The peaks at 1735, 1641, 1194 and 1023 cm^{-1} that appeared in all samples from C-3 to C-12 were attributed to vibrations of C=O, N-H, C-O and Ti-O bonds separately, and all peaks were dimmed out with prolonged heating time. It must be pointed out that the peaks at 1075 and 1370 cm^{-1} of sample C-3 belonging to C-O and C-N stretching vibrations shifted to 1115 and 1400 cm^{-1} in the following samples from C-6 to C-12, which probably meant further interactions between CDs and TiO_2. Compared with the FTIR spectrum of pure CDs, it's easy to find that almost all the characteristic peaks of the CDs-TiO_2 composites could be found in the lineshape of CDs (Fig. S6). Whereas there were two stable characteristic peaks at 1633 and 1400 cm^{-1} corresponding to C=C and C-N vibrations appeared in all samples from C-400 to C-550. Obviously, the solvothermal process was a mild approach to obtain CDs-TiO_2 composites with abundant groups on the surface besides the fine hybridization. While the further calcination realized the finely doping of inert carbon and TiO_2, as most of surface functional groups were sacrificed in the calcination.

Further characterization studies using XPS provided convincing evidences for the surface states and composition of the as-prepared samples and the results were illustrated in Fig. 5. Both sample C-9 and C-450 showed clear constituents of element C, O and Ti. To be particularly, though the high-resolution C 1s spectra (Fig. 5b and Fig. 5e) showed a similar distribution of signals, the intensity of each signal differed observably. The strongest signal of sample C-9 emerged at 286.1 eV attributing to C=O and C-N, while that of C-450 was found at 284.9 eV corresponding to C-O and graphite carbon. It's easy to conclude that the functional groups on the surface of sample C-450 were less than that of C-9 as a result of the further calcination. In fact, a 42.2 % and 28.9 % C atomic content were detected respectively from C-9 and C-450, indicating a sharp decrease of C contents in the samples. Especially to sample C-9, detection of a 4.3 % N atomic content further confirmed the successful N-doping in the CDs-TiO_2 composites. However, most N-doping were probably accompanied with CDs, for the N1s peak (400 eV around) of sample C-450 almost vanished, leaving a very unapparent lineshape, which meant a very low N content. Whether or not, the high-resolution Ti 2p spectra (Fig. 5c and Fig. 5f) of sample C-9 and C-450 held same signals all through at 458 eV and 464 eV around, attributing to the atomic state of Ti-O.

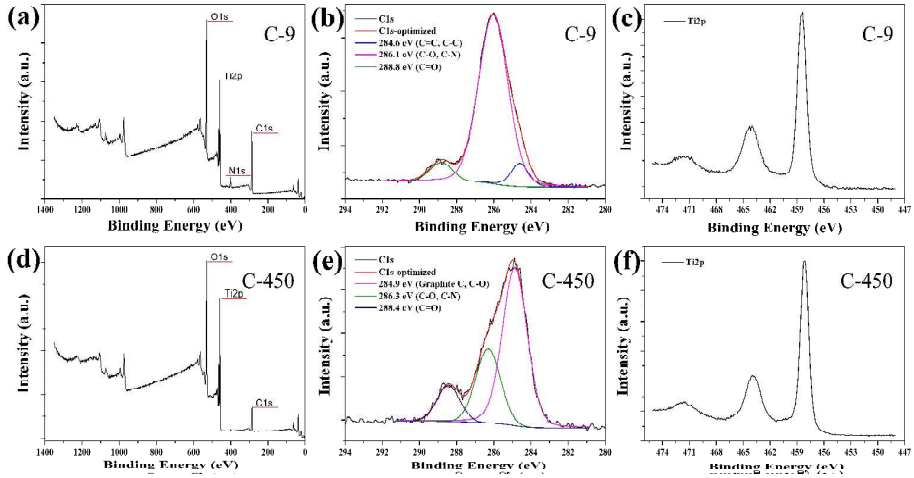

Fig. 5 XPS spectra of sample C-9 (a, b c) and C-450 (d, e, f).

The detailed PL properties of pure CDs were studied by changing excitation wavelengths ranging from 360 to 500 nm (Fig. 6). With the increase of the excitation wavelength, the maximum emission peak position shifted to longer wavelength gradually, accompanied with remarkable decrease of PL intensity. This phenomenon was accordant with that observed by Zhang[34], which meant the photoexcited charge carriers could be generated by the visible light, attributing to the complex surface states of CDs. And the droplet containing CDs exhibited blue, green and red photoluminescence, respectively, under ultraviolet (330 – 385 nm), blue (460 – 495 nm) and green (530 – 550 nm) light excitation. Likewise, powders of sample C-9 showed clear blue, green and red photoluminescence compared with C-450 and pure TiO_2 under the same photograph conditions (Fig. S7), indicating that CDs were abundant and well-distributed in the CDs-TiO_2 composites. However, the upconverted PL property of CDs, which was regarded as an important causation to improve the photocatalytic activity of TiO_2 mentioned by Lee[32] and Liu[35], was not found here.

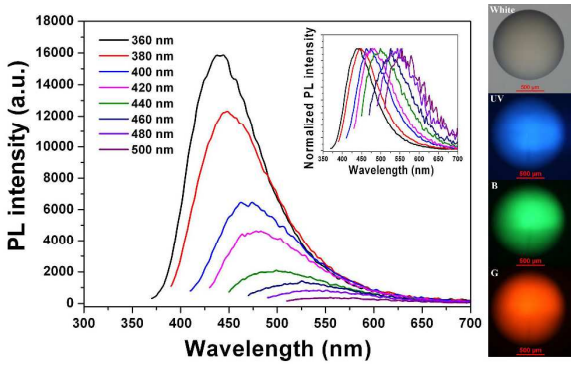

Fig. 6 PL emission spectra of the pure CDs (left) and fluorescent microscopy images of diluted aqueous solution containing CDs under white, ultraviolet (330 – 385 nm), blue (460 – 495 nm) and green (530 – 550 nm) light excitation (right).

To further determine the possible constituents of the as-prepared composites, concentrated sulfuric acid was used to dissolve the samples. As shown in Fig. S8, both sample C-9 and P25 could be dissolved completely, forming a transparent solution separately but with different colors. However, we could only get a suspension for sample C-450 even using the hot concentrated sulfuric acid. Furthermore, these obtained solutions were examined under a UV lamp with emission wavelengths centered at 365 nm (Fig. S9). Obvious fluorescence could be found from the solution in which sample C-9 was dissolved. Then the suspension of sample C-450 emitted a relatively weak fluorescent light too. As for P25, no fluorescence was observed at all. These results reconfirmed that sample C-9 was a nanohybrid of CDs and TiO_2, and most CDs were converted into inert and insoluble carbon materials in sample C-450 after the calcination.

In order to investigate the special chemical properties of the as-prepared composites, we firstly evaluated their photocatalytic ability for the photo-degradation of MB under UV light (254 nm), comparing with the pure TiO_2 (Degussa P25). It had been proved that the UV-vis absorbance at 664 nm was liner with the concentration of MB solutions (Fig. S10), especially when the concentration was no more than 10 ppm. Fig. 7 plotted the UV-vis absorption curves of the reaction solutions at regular intervals, representing the photocatalytic ability of different catalysts. We can see that when a 10 min irradiation of UV light was carried out on the 10 ppm MB solution containing sample C-9, decontamination of MB was almost complete (ca. 95%). In fact, all the CDs-TiO_2 composites were efficient on photo-degradation of MB under UV light (Fig. S11), and sample C-9 was the best one. In the control experiment, using sample C-450 as catalysts, the degradation rate of MB was about 37% after 10 min irradiation. And a complete photo-degradation of MB (ca. 96%) for C-450 required 40 min of UV light irradiation. Compared with the other C-TiO_2 composites, C-450 showed the best photocatalytic ability, following by sample C-500 (Fig. S12). While under the same conditions, reduction of MB was only 72% even after 40 min irradiation to the pure TiO_2. These results indicated that CDs-TiO_2 composites could be served as an efficient photocatalyst for MB. Moreover, in order to check the recyclability of the catalysts, we repeated the above catalytic tests but using a timesaving concentration of MB (5 ppm). The intensity ratios of the absorbance at 664 nm after and prior to the UV light irradiation for a certain time (A/A_0) were plotted as a function of the reaction time. It was found that there was no significant drop of the photocatalytic efficiency even after ten cycles for sample C-9, and all the photo-degradation processes were finished in 10 min, which meant that the CDs-TiO_2 composites had great potential for practical application. While in the control experiment, as shown in Fig. 7d, though there was a 10% around drop of the photocatalytic efficiency after ten cycles for sample C-450 with a 20 min irradiation, the photo-degradation processes were completed after 40 min of UV light irradiation. As to the pure TiO_2, it was too difficult to collect all the powders of P25 after the photo-degradation trials, let alone the recycling for next photocatalysis.

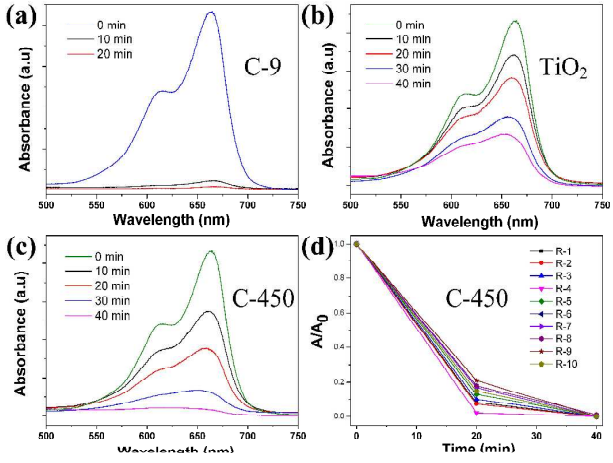

Fig. 7 UV-vis absorption spectra monitoring the degradation of MB (a, b, c) and cycling tests of photocatalytic activity of sample C-450 (d).

To further explore the photocatalytic activity of the as-prepared composites, MO and RB were also used as the mimetic pollutants. As shown in Fig. S13, after a 60 min irradiation under UV light, 56% and 82% of MO were degraded by the sample C-9 and C-450, separately. It was interesting that this time sample C-450 is

more efficient on photo-degradation of MO. Furthermore, lower photocatalytic efficiency (ca. 34%) was achieved by sample C-9 to degrade RB, comparing to 88% of C-450. That is to say, the CDs-TiO_2 composites were good at the photo-degradation of MB. As to MO and RB, the C-TiO_2 composites exhibited more advantages.

During the photocatalysis, three factors are crucial, including the adsorption of reactants, the light absorption, and the charge separation and transportation. The adsorption capacity of sample C-9 and C-450 was roughly tested upon MB, MO and RB. The absorbance measured at the adsorption-desorption equilibrium was contrasted with that of the original solution (Shown in Fig. S14). Sample C-450 showed a slight adsorption upon all the pollutants. It was similar for sample C-9 upon MO and RB. However, MB was seriously absorbed by sample C-9. The effect of this absorption on the photocatalytic ability of sample C-9 was further explored. As shown in Fig. S15, the absorbance at the adsorption-desorption equilibrium in each cycle was measured without irradiation. The MB concentration increased along with the number of equilibrium cycles. Several cycles were chosen to test the photocatalytic ability of sample C-9 after absorption of considerable amounts of MB. Though 48% MB was absorbed by sample C-9 at the adsorption-desorption equilibrium of sixth cycle, photo-degradation of MB was still up to 91% after 10 min irradiation. The figure dropped to 64% in test of eighth cycle. While in the eighteenth cycle, the photocatalytic efficiency was only 46% after 20 min irradiation. It was reconfirmed that the CDs-TiO_2 composites were efficient on photo-degradation of MB, besides a special absorption capability for MB. However, the photocatalytic activity would be weakened if too many MB were absorbed.

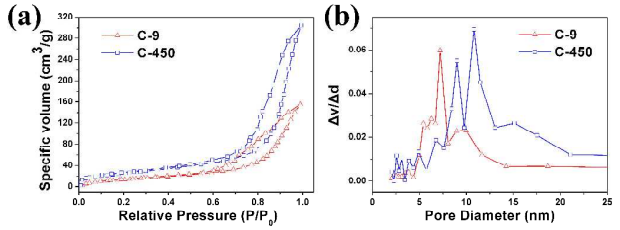

Fig. 8 Nitrogen adsorption-desorption isotherms (a) and pore size distribution curves (b) of sample C-9 and C-450.

As the adsorption of reactants usually was dependent on structural or surface characteristics of the catalysts, the structural characteristics of prepared samples here were further analyzed by nitrogen adsorption-desorption isotherm, as shown in Fig. 8a. Both of the isotherms were of type IV (BDDT classification). At high relative pressures from 0.6 and 1.0, the isotherms exhibited hysteresis loops of type H_3, indicating that the two samples contained mesopores (2 - 50 nm). But evidently, the specific volume of adsorbed nitrogen molecules increased sharply for sample C-450 with enhanced relative pressure of nitrogen. And the BET specific surface areas calculated for sample C-450 was 92.7 m^2 g^{-1}, comparing to a value of 55.5 m^2 g^{-1} for sample C-9. Fig. 8b showed the corresponding pore size distribution curves. The pore diameters of sample C-9 and C-450 were 7.0 nm and 10.5 nm, respectively. In other words, sample C-450 possessed higher BET specific surface area and bigger pore diameter than that of C-9. This might be caused by the further carbonization and reactions in the CDs-TiO_2 composites brought forth by the calcination. It's known that the BET specific surface area of commercial pure TiO_2 (P25) was 50.0 m^2 g^{-1} around, which was close to that of sample C-9. Combined with the above photcatalytic results, it could be speculated that the superior adsorption of MB for the CDs-TiO_2 composites did not only stem from their big specific surface areas, but also probably from the microporous structure and aboundant surface functional groups introduced by CDs. However, it seemed that the superior adsorption of CDs-TiO_2 composites functioned on MB only. As to MO and RB, the big specific surface areas and proper proportion of anatase/rutile content of the C-TiO_2 composites were more advantageous.

Here, we conjectured that the introduction of CDs, together with fine nano-hybrid of CDs and TiO_2, may be responsible for their excellent photocatalytic performance on MB. And the underlying causes for the enhanced photocatalytic property of the CDs-TiO_2 composites were presumed as follows. Firstly, the programmed preparation process induced microporous structure and abundant functional groups were beneficial to adsorption of reactants as soon and much as possible. Secondly, as a carbon material at the nanoscale, CDs could well accept the photogenerated electrons from TiO_2 and promote the separation of photogenerated charge carriers. Lastly, the nano-hybrid and tight integration of CDs and TiO_2 could help for the transfer of photogenerated electrons efficiently, and then reduce the recombination rate of electron-hole pairs greatly. As to the C-TiO_2 composites, though most CDs lost in the calcination, the rest CDs and new amorphous carbon, the bigger specific surface areas and proper proportion of anatase/rutile content, all together contributed to the final excellent photocatalytic activity.

Conclusion

The CDs-TiO_2 composites were successfully synthesized in situ via a one-step solvothermal route. And the doping of CDs and TiO_2 particles was achieved at the nanoscale under our programmed experiments. Moreover, the final CDs-TiO_2 composites were of a "microsphere" shape, which was advantaged in separation off the reaction system after photocatalysis. The crystallinity of TiO_2, ingredients, microstructure and surface state of CDs-TiO_2 composites could be adjusted by the reaction time. Though CDs here didn't show the upconverted PL property, it was sensitive to light in a quite broad range, especially to UV light. The photo-degradation of MB showed excellent photocatalytic activity of the CDs-TiO_2 composites, which was much higher than that of commercial Degussa P25. It's believed that nanohybird of CDs and TiO_2, together with the chemical and optical properties introduced by CDs, made most contributions to the enhanced photocatalytic activity of the CDs-TiO_2 composites. Furthermore, C-TiO_2 composites were produced from the CDs-TiO_2 composites by a further calcination, which had shown a more excellent photocatalytic activity on the photo-degradation of MO and RB. Besides the effects of CDs, the newly generated amorphous carbon that finely doped with TiO_2, bigger specific surface areas and proper proportion of anatase/rutile content, probably accounted for the enhanced photocatalytic activity of the C-TiO_2 composites.

Acknowledgements

The authors gratefully acknowledge the support for this work from the National Natural Science Foundation of China (Grant 51303210 and 51202292) and National Science and Technology Major Project of China (Grant 2012ZX10004801-003).

Notes and references

Institute of Medical Equipment, Academy of Military Medical Sciences, Tianjin 300161, PR China. Email: tianfeng62037@163.com.

†Electronic Supplementary Information (ESI) available: Experimental details and supplementary data. See DOI: 10.1039/b000000x/

1 X. B. Chen, S. H. Shen, L. J. Guo and S. S. Mao, *Chem. Rev.*, 2010, **110**, 6503-6570.
2 G. Li, L. Wu, F. Li, P. Xu, D. Zhang and H. Li, *Nanoscale*, 2013, **5**, 2118-2125.
3 Z. X. Li, Y. L. Xie, H. Xu, Y. M. Wang, Z. G. Xu and H. L. Zhang, *J. Photochem. Photobiol.*, A, 2011, **224**, 25-30.
4 H. Kim, J. Kim, W. Kim and W. Choi, *J. Phys. Chem. C*, 2011, **115**, 9797-9805.
5 S. Liu, E. Guo and L. Yin, *J. Mater. Chem.*, 2012, **22**, 5031-5041.
6 P. Xu, T. Xu, J. Lu, S. Gao, N. S. Hosmane, B. Huang, Y. Dai and Y. Wang, *Energy Environ. Sci.*, 2010, **3**, 1128-1134.
7 M. Yang, H. Jha, N. Liu and P. Schmuki, *J. Mater. Chem.*, 2011, **21**, 15205-15208.
8 K. E. deKra, C. Wang and W. B. Lin, *Adv. Mater.*, 2012, **24**, 2014-2018.
9 G. Halasi, G. Schubert and F. Solymosi, *J. Catal.*, 2012, **294**, 199-206.
10 J. Wang and Z. Lin, *Chem. Mater.*, 2010, **22**, 579-584.
11 Y. Park, S. H. Lee, S. O. Kang and W. Choi, *Chem. Commun.*, 2010, **46**, 2477-2479.
12 T. T. Le, M. S. Akhtar, D. M. Park, J. C. Lee and O. B. Yang, *Appl. Catal., B*, 2012, **111-112**, 397-401.
13 P. A. DeSario, J. J. Pietron, D. E. DeVantier, T. H. Brintlinger, R. M. Stroud and D. R. Rolison, *Nanoscale*, 2013, **5**, 8073-8083.
14 B. Liu, Q. Wang, S. Yu, P. Jing, L. Liu, G. Xua and J. Zhang, *Nanoscale*, 2014, **6**, 11887-11897.
15 N. Zhang, S. Liu and Y. J. Xu, *Nanoscale*, 2012, **4**, 2227-2238.
16 G. S. Wu, J. P. Wang, D. F. Thomas, A. C. Chen, *Langmuir*, 2008, **24**, 3503-3509.
17 R. Asahi, T. Morikawa, T. Ohwaki, K. Aoki and Y. Taga, *Science*, 2001, **293**, 269-271.
18 S. U. M. Khan, M. A. Shashry and W. B. Ingler Jr, *Science*, 2002, **297**(5590), 2243-2245.
19 S. Sakthivel and H. Kisch, *Angew. Chem., Int. Ed.*, 2003, **42**, 4908-4911.
20 T. Ohno, M. Akiyoshi, T. Umebayashi, K. Asai, T. Mitsui and M. Matsumura, *Appl. Catal., A*, 2004, **265**, 115-121.
21 J. C. Yu, J. Yu, W. Ho, Z. Jiang, L. Zhang, *Chem. Mater.*, 2002, **14**, 3808-3816.
22 S. In, A. Orlov, R. Berg, F. Garcı´a, S. Pedrosa-Jimenez, M. S. Tikhov, D. S. Wright, R. M. Lambert, *J. Am. Chem. Soc.*, 2007, **129**, 13790-13791.
23 X. Chen, L. Liu, P. Y. Yu and S. S. Mao, *Science*, 2011, **331**, 746-750.
24 Y. Yan, M. Han, A. Konkin, T. Koppe, D. Wang, T. Andreu, G. Chen, U. Vetter, J. R. Morante and P. Schaaf, *J. Mater. Chem. A*, 2014, **2**, 12708-12716.
25 G. C. Xie, K. Zhang, B. D. Guo, Q. Liu, L. Fang and J. R. Gong, *Adv. Mater.*, 2013, **25**, 3820-3839.
26 N. Zhang, Y. H. Zhang and Y. J. Xu, *Nanoscale*, 2012, **4**, 5792-5813.
27 H. I. Kim, G. H. Moon, D. M. Satoca, Y. Park and W. Choi, *J. Phys. Chem. C*, 2012, **116**, 1535-1543.
28 S. T. Kochuveedu, Y. J. Jang, Y. H. Jang, W. J. Lee, M. A. Cha, H. Shin, S. Yoon, S. S. Lee, S. O. Kim, K. Shin, M. Steinhart and D. H. Kim, *Green Chem.*, 2011, **13**, 3397-3405.
29 G. Zhang, F. Teng, Y. Wang, P. Zhang, C. Gong, L. Chen, C. Zhao and E. Xie, *RSC Adv.*, 2013, **3**, 24644.
30 S. Wang, L. Zhao, L. Bai, J. Yan, Q. Jiang and J. Lian, *J. Mater. Chem. A*, 2014, **2**, 7439-7445.
31 S. N. Baker and G. A. Baker, *Angew. Chem. Int. Ed.*, 2010, **49**, 6726-6744.
32 H. Li, X. He, Z. Kang, H. Huang, Y. Liu, J. Liu, S. Lian, C. H. A. Tsang, X. Yang and S.-T. Lee, *Angew. Chem.*, 2010, **49**, 4430-4434.
33 J. Wang, M. Gao and G. W. Ho, *J. Mater. Chem. A*, 2014, **2**, 5703-5709.
34 L. Feng, X. Y. Tang, Y. X. Zhong, Y. W. Liu, X. H. Song, S. L. Deng, S. Y. Xie, J. W. Yan and L. S. Zheng, *Nanoscale*, 2014, **6**, 12635-12643.
35 X. Yu, J. Liu, Y. Yu, S. Zuo, B. Li. *Carbon*, 2014, **68**, 718-724.
36 J. Bian, C. Huang, L. Wang, T.F. Hung, W. A. Daoud, and R. Zhang, *ACS Appl. Mater. Interfaces*, DOI: dx.doi.org/10.1021/am4059183.
37 S. Xie, H. Su, W. Wei, M. Li, Y. Tong and Z. Mao, *J. Mater. Chem. A*, 2014, **2**, 16365-16368.
38 M. Sun, X. Ma, X. Chen, Y. Sun, X. Cui and Y. Lin, *RSC Adv.*, 2014, **4**, 1120-1127.
39 Z. Jiang, W. Wei, D. Mao, C. Chen, Y. Shi, X. Lv and J. Xie, *Nanoscale*, 2015, **7**, 784-797.
40 J. Liu, W. Zhu, S. Yu, X. Yan, *Carbon*, 2014, **79**, 369-379.
41 Z. Ma, H. Ming, H. Huang, Y. Liu and Z. Kang, *New J. Chem.*, 2012, **36**, 861-864.
42 X. Zhang, F. Wang, H. Huang, H. Li, X. Han, Y. Liu and Z. Kang, *Nanoscale*, 2013, **5**, 2274-2278.
43 J. Zhong, F. Chen and J. Zhang, *J. Phys. Chem. C*, 2010, **114**, 933-939.